Rational design of open hollow nanoboxes via Ru and B synergistic electronic modulation in cobalt phosphide for efficient oxygen evolution reaction

Zhao Li,[a] Wenjing Cheng,[a] Xuena Gao,[a] Chunmei Ni,[a,c] Jianguo Dong,[a] Huiming Yang,[a] Ju Wang,[a] Wenyi Tan,[a] and Lin Tian [a,b,c]*

[a]School of Materials and Chemical Engineering, Xuzhou University of Technology, Xuzhou 221018, PR China

[b]University and College Key Lab of Natural Product Chemistry and Application in Xinjiang, School of Chemistry and Environmental Science, Yili Normal University, Yining 835000, China.

[c]Key Laboratory of Advanced Catalytic Materials and Technology, Advanced Catalysis and Green Manufacturing Collaborative Innovation Center, Changzhou University, Changzhou, Jiangsu Province 213164, China

Corresponding author: Tel: 86-516-83105518

Email: xzittl@xzit.edu.cn (L. Tian)

1. Electrochemical Measurements

All tests were conducted using a CHI760E electrochemical workstation in a three-electrode configuration with 1.0 M KOH as the electrolyte. A glassy carbon electrode (GCE) loaded with catalyst, a carbon rod, and a Hg/HgO electrode were used as the working, counter, and reference electrodes, respectively. All potentials were converted to the reversible hydrogen electrode (RHE) scale using $E(RHE) = E(Hg/HgO) + 0.098 + 0.059 \times pH$. Current densities were normalized to the geometric area of the GCE.

Catalyst ink was prepared by dispersing 5 mg catalyst in a mixture of 780 μL ethanol, 200 μL water, and 20 μL 5 wt% Nafion, followed by 1 h sonication. Commercial IrO_2 ink was prepared similarly. For OER tests, the catalyst was activated via 50 cyclic voltammetry (CV) cycles at 30 mV/s. Linear sweep voltammetry (LSV) was performed at 5 mV/s. Tafel plots were derived from η vs. log(j). All LSV and Tafel data were iR-compensated (95%). Electrochemical impedance spectroscopy (EIS) was measured at $\eta = 0.3$ V from 10 kHz to 0.01 Hz. Double-layer capacitance (Cdl) was determined from CV scans at 10-80 mV/s in a non-faradaic region. The electrochemical active surface area (ECSA) was calculated as $ECSA = C_{dl} / Cs$, where $Cs = 0.04$ mF/cm^2. Turnover frequency (TOF) was calculated using $TOF = (j \times NA) / (4 \times n \times F)$, where n is the number of active sites.

2. Density Functional Theory Calculations

A Ru atom was doped into the thermodynamically stable CoP (111) surface—selected as the catalytic platform for its exposure of high-activity Co sites—while B and N were doped into the carbon layer. For Ru doping in the CoP lattice, the most stable doped structure was identified by systematically evaluating different occupancy configurations of Ru; the doped Ru atom was precisely positioned near adsorption sites to clarify its influence on OER intermediates. Furthermore, in this study, the control

variable method was adopted, and a single Ru atom was selected for doping to ensure the rigor of comparisons with undoped systems. Regarding the B/N co-doped carbon matrix, boron doping was confirmed to be uniformly distributed within the NC matrix, supported by signals of B-N and B-C bonds in the B 1s spectrum, the characteristic peak of graphitic N in the N 1s spectrum, and the presence of C-B and C-N bonds in the C 1s spectrum. Through this approach, Ru doping in the CoP lattice and B/N co-doping in the carbon layer were integrated to form the target heterostructure.

The OER process was modeled via four sequential proton-coupled electron transfer steps, following the elementary reactions:

$$OH^- + * \rightarrow OH^* + e^- \quad (1)$$

$$OH^* + OH^- \rightarrow O^* + H_2O + e^- \quad (2)$$

$$O^* + OH^- \rightarrow OOH^* + e^- \quad (3)$$

$$OOH^* + OH^- \rightarrow O_2 + * + H_2O + e^- \quad (4)$$

The adsorption energies (ΔE_{ads}) of the OH*, O*, and OOH* intermediates were calculated by referencing the total DFT energies and gas-phase H_2O and H_2. The corresponding adsorption free energies (ΔG_{ads}) were determined using the expression: $\Delta G_{ads} = \Delta E_{ads} + \Delta ZPE - T\Delta S$, where ΔZPE and ΔS represent the zero-point energy and entropy contributions, respectively. For each OER step, the Gibbs free energy change was evaluated according to:$\Delta G = \Delta E_{DFT} + \Delta ZPE - T\Delta S - eU$, where ΔE_{DFT} is the reaction energy from DFT calculations, and U is the applied electrode potential with reference to the standard hydrogen electrode (SHE), while e denotes the number of electrons transferred.

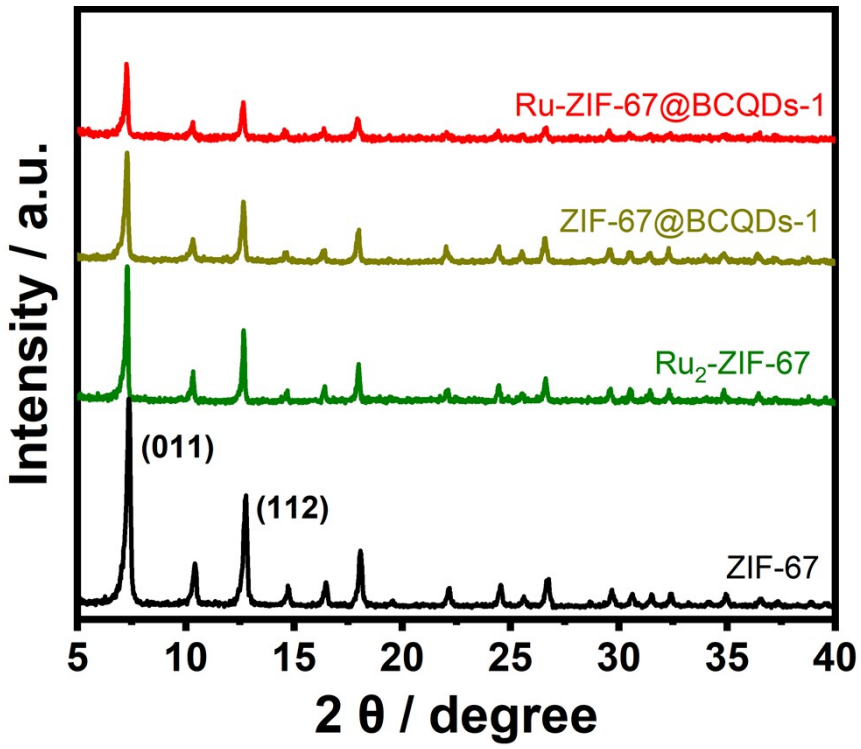

Fig. S1 The XRD pattern of ZIF-67, Ru_2-ZIF-67, ZIF-67@BCQDs-1, and Ru-ZIF-67@BCQDs-1.

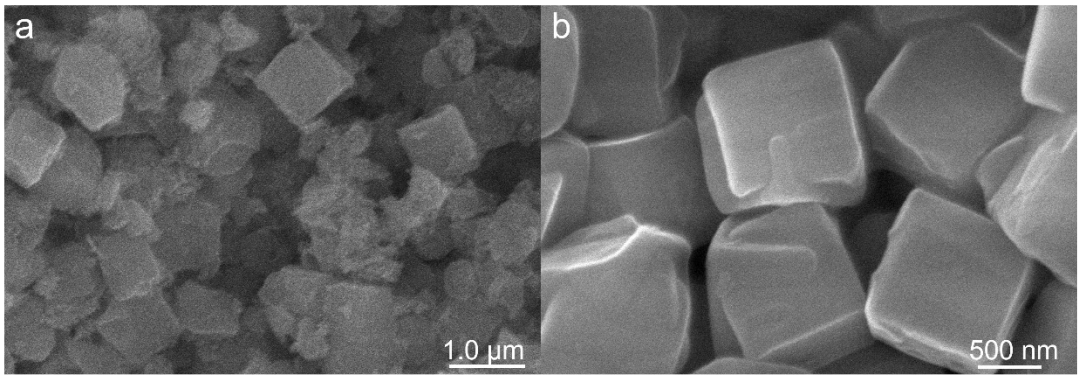

Fig. S2 SEM images of (a) ZIF-67@BCQDs-1 and (b) Ru_2-ZIF-67.

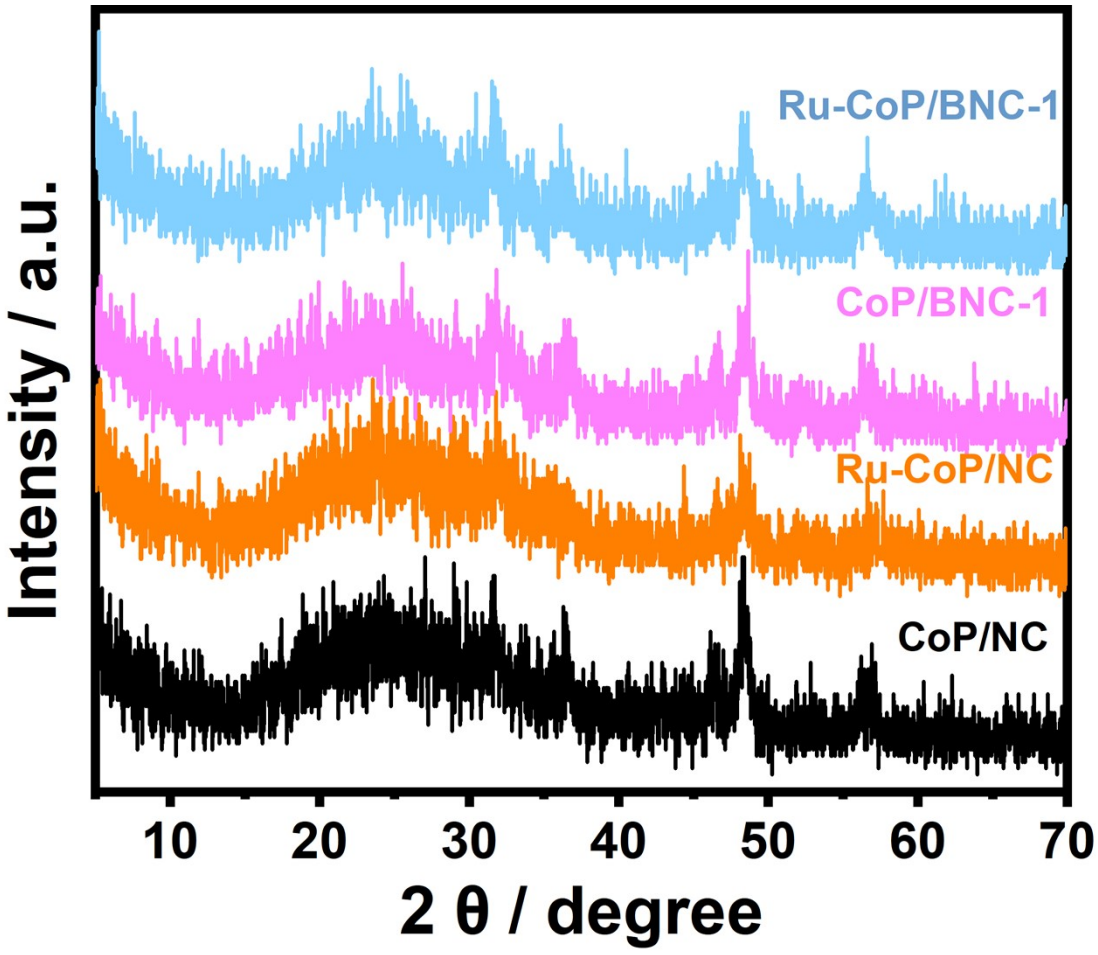

Fig. S3 The XRD pattern of various samples.

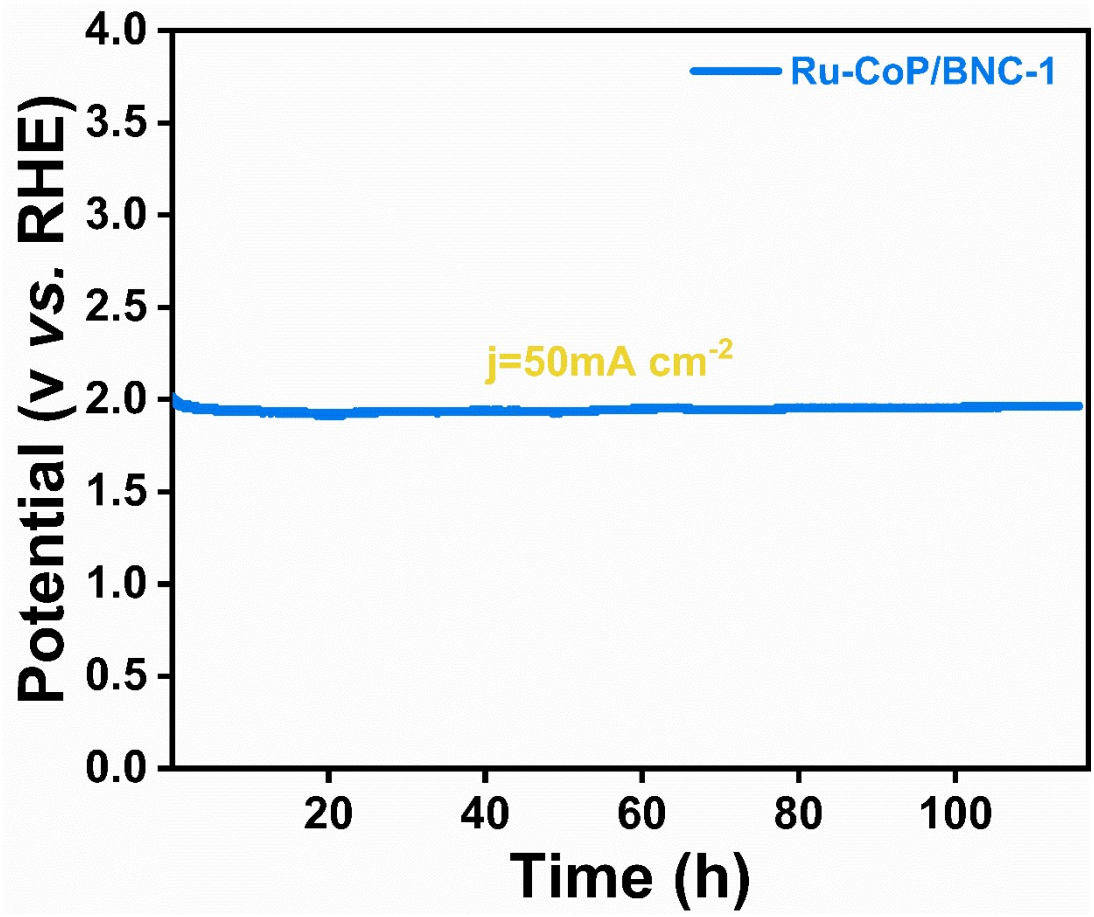

Fig. S4 Prolonged CP of Ru-CoP/BCN-1 at 50 mA cm^{-2}.

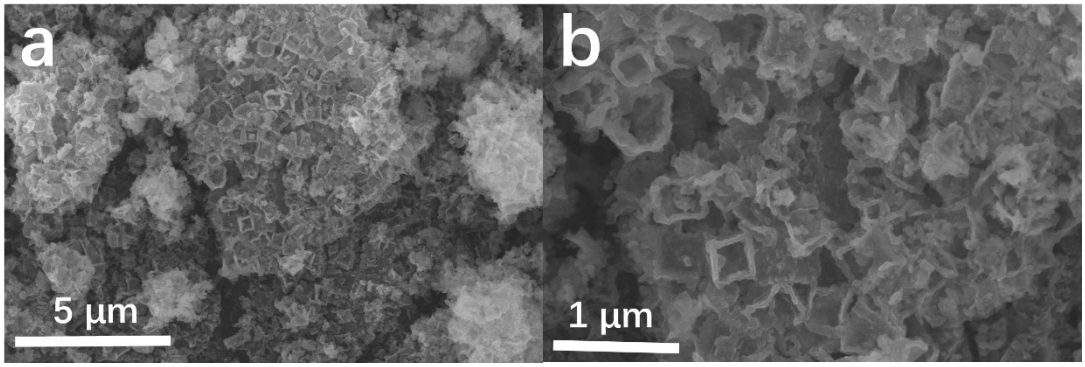

Fig. S5 (a, b) SEM images of Ru-CoP/BNC-1 after OER at different magnifications.

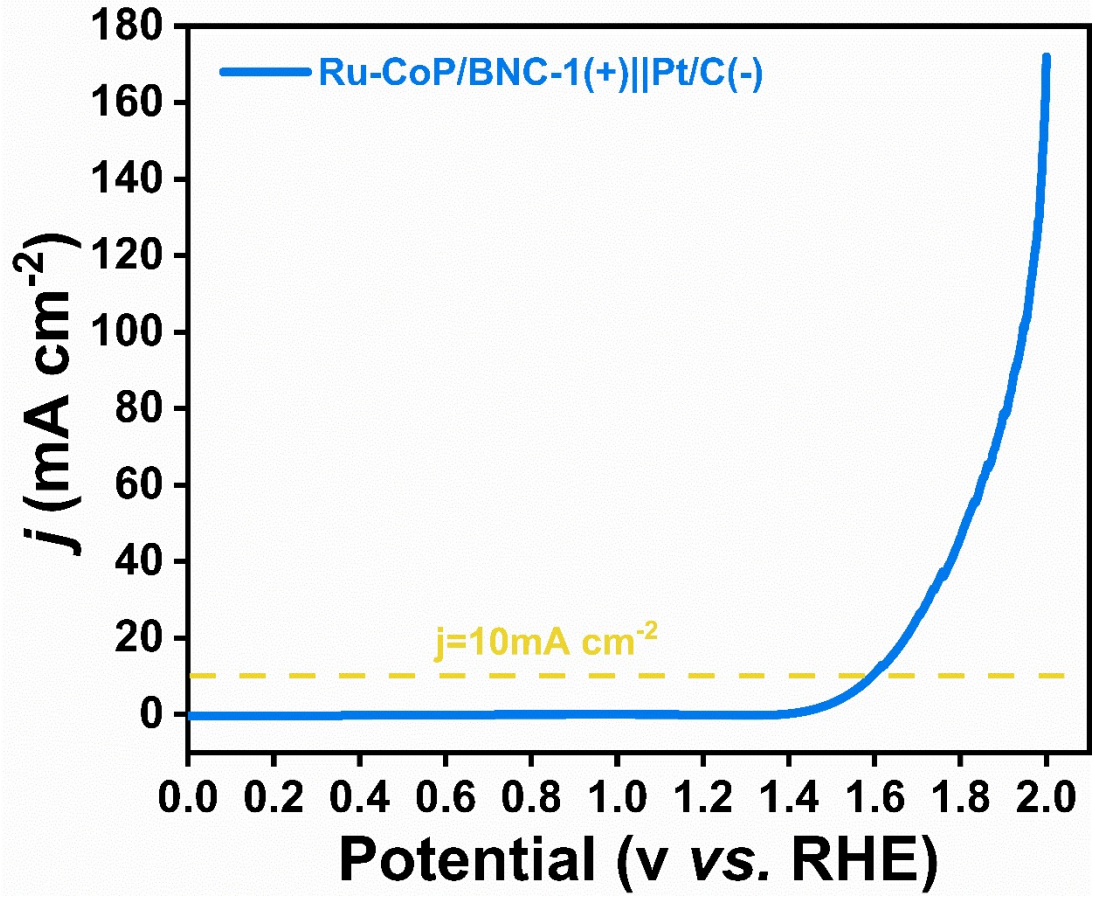

Fig. S6 LSV polarization curve of Ru-CoP/BNC-1(+)||Pt/C(-).

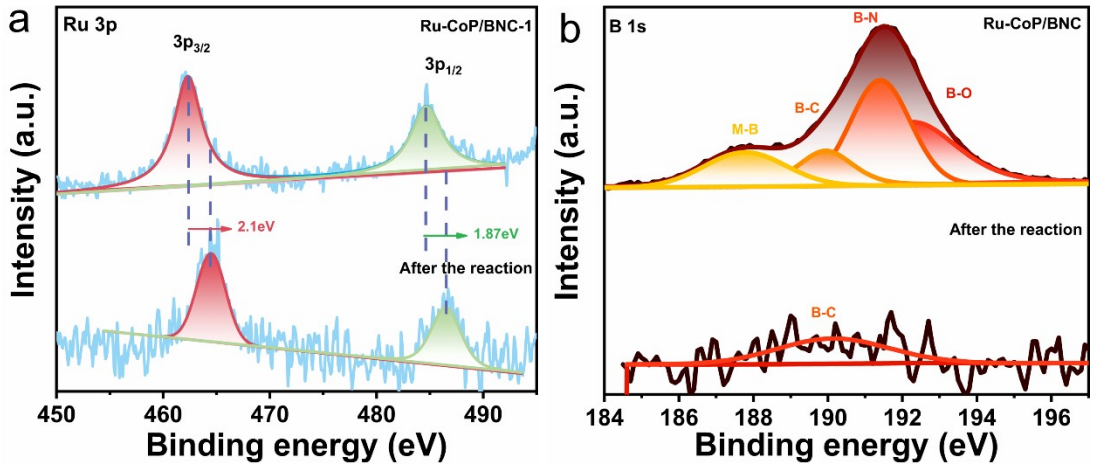

Fig. S7 (a) Ru 3p and (b) B 1s XPS spectra of Ru-CoP/BNC-1 before and after OER.

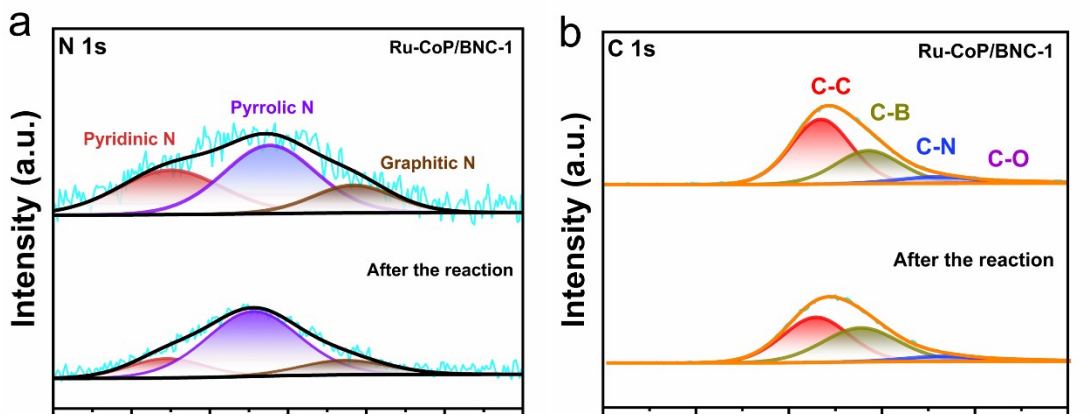

Fig. S8 (a) N 1s and (b) C 1s XPS spectra of Ru-CoP/BNC-1 before and after OER.

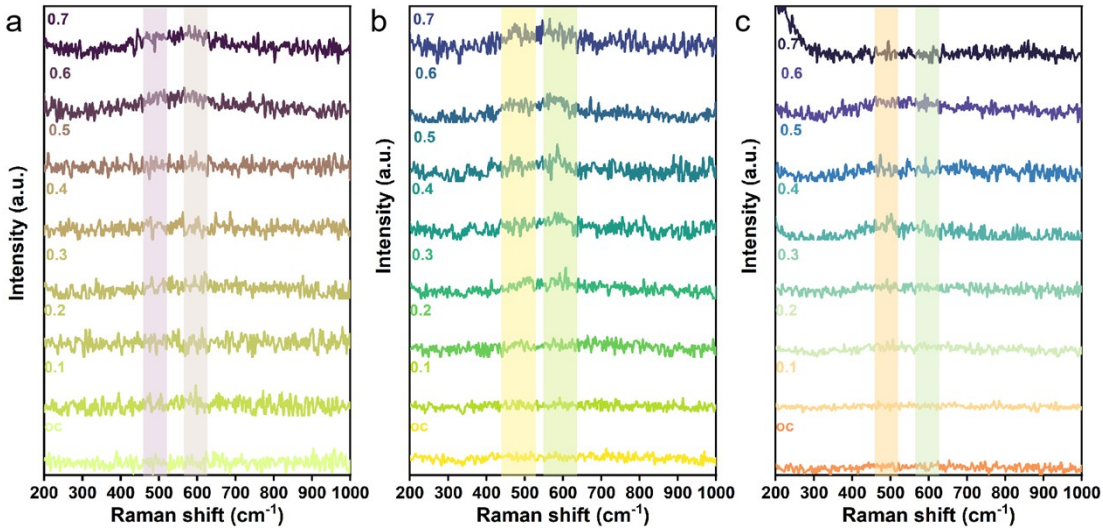

Fig. S9 In situ Raman spectra of (a) Ru-CoP/NC, (b) CoP/BNC-1, (c) CoP/NC.

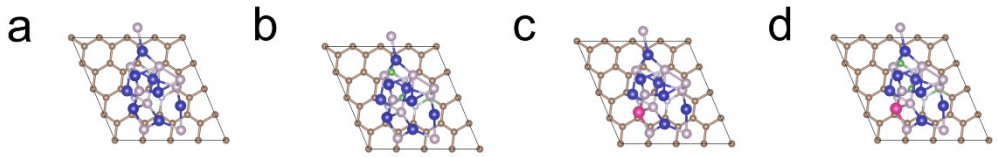

Fig. S10 Top views of (a) CoP/NC, (b) CoP/BNC-1, (c) Ru-CoP/NC, and (d) Ru-CoP/BNC-1.

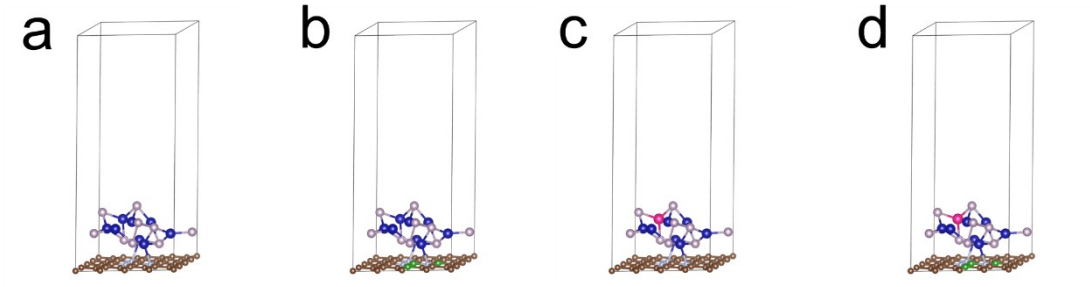

Fig. S11 Side views of (a) CoP/NC, (b) CoP/BNC-1, (c) Ru-CoP/NC, and (d) Ru-CoP/BNC-1.

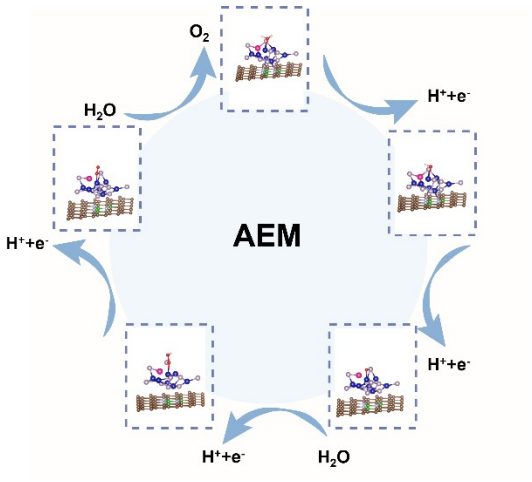

Fig. S12 Schematic illustration of the oxygen evolution reaction (OER) pathway on Ru-CoP/BNC-1.

Compounds	I_{011}/I_{211}
ZIF-67	1.88
Ru_2-ZIF-67	1.84
ZIF-67@BCQDs-1	1.48
Ru-ZIF-67@BCQDs-1	1.76

Table S1 The intensity ratio of the (011) and (211) crystal planes in various samples.

	Ru-CoP/BNC-0.33	Ru-CoP/BNC-1	Ru-CoP/BNC-3	Ru-CoP/NC	CoP/BNC-1	CoP/NC	RuO_2
10mA cm^{-2}	260	227	271	274	299	317	295
20mA cm^{-2}	297	276	312	320	333	354	328
50mA cm^{-2}	341	332	362	375	374	/	/

Table S2 Overpotentials at different current densities.

	Rs	Rw	Q1	Q2	Rct
Ru-CoP/BNC-0.33	8.801	2.689	$1.756*10^{-5}$	$4.881*10^{-3}$	40.32
Ru-CoP/BNC-1	0.002182	12.07	$3.457*10^{-3}$	$8.702*10^{-3}$	27.56
Ru-CoP/BNC-3	10.56	4.815	$2.891*10^{-4}$	$7.655*10^{-4}$	114.5
Ru-CoP/NC	6.922	7.295	$2.633*10^{-4}$	$1.154*10^{-3}$	133
CoP/BNC-1	9.828	11.69	$6.054*10^{-4}$	$1.011*10^{-3}$	162
CoP/NC	7.103	6.924	$3.187*10^{-4}$	$1.125*10^{-3}$	179.5

Table S3 Simulated impedance values for various parts.